SUMER SPECTRAL OBSERVATIONS OF POST-FLARE SUPRA-ARCADE INFLOWS

D. E. INNES[1], D. E. McKENZIE[2] and TONGJIANG WANG[1]
Max-Planck-Institut für Aeronomie, Max-Planck-Str. 2, 37191 Katlenburg-Lindau, Germany
(e-mail: innes@linmpi.mpg.de)
[2]*Department of Physics, Montana State University, P.O. Box 173840, Bozeman, Montana 59717-3840, U.S.A.*

(Received 13 March 2003; accepted 18 July 2003)

Abstract. On 21 April 2002 a large eruptive flare on the west limb of the Sun developed a bright, very dynamic, post-flare arcade. In TRACE 195 Å images, a series of dark, sunward moving flows were seen against the bright extreme ultraviolet (EUV) arcade. SUMER obtained a series of spectra of the dark EUV flows in the lines C II, Fe XII, and Fe XXI at a fixed position above the limb. These spectra give spatially resolved line-of-sight velocities and emission measures for the arcade plasma over a temperature range 2×10^4 to 10^7 K. The flows are dark in all SUMER lines. The UV continuum longward ($\sim$1350 Å) and shortward ($\sim$675 Å) of the hydrogen Lyman limit is used to determine whether the dark 195 Å inflows are due to regions of low plasma density (plasma voids) or cold absorbing material. There is some evidence of absorption near the front of one of the inflows; however, along most of the dark channels there is no change in continuum ratio and we therefore conclude, as originally suggested by McKenzie and Hudson (1999), that they are plasma voids.

1. Introduction

Large structures above postflare soft X-ray arcades (supra-arcade structures) rising over 200 Mm into the solar corona have been seen and described for a number of long-duration solar flares. The supra-arcade structures look like fans of coronal rays directed outwards into the corona from the top of what appears to be a typical postflare loop system. In several of the supra-arcade events sunward moving structures have been seen in *Yohkoh*/SXT images (McKenzie and Hudson, 1999; McKenzie, 2000). All events with sunward flow are associated with large coronal mass ejection (CME) events. The majority of these flows look like dark trails falling from the corona through the flare arcade toward the Sun. They seem to slow and stop as they reach the height of the main arcade flare loops. From their appearance and their association with CMEs one may think that the sunward flows are ejected chromospheric material falling back to the Sun; however, so far not a single one of them has been seen in Hα emission or cold line images. McKenzie and Hudson (1999) and McKenzie (2000) suggested, after analyzing soft X-ray images, that they are cross sections of evacuated flux tubes (plasma voids) contracting down to their equilibrium position.

Solar Physics **217:** 247–265, 2003.

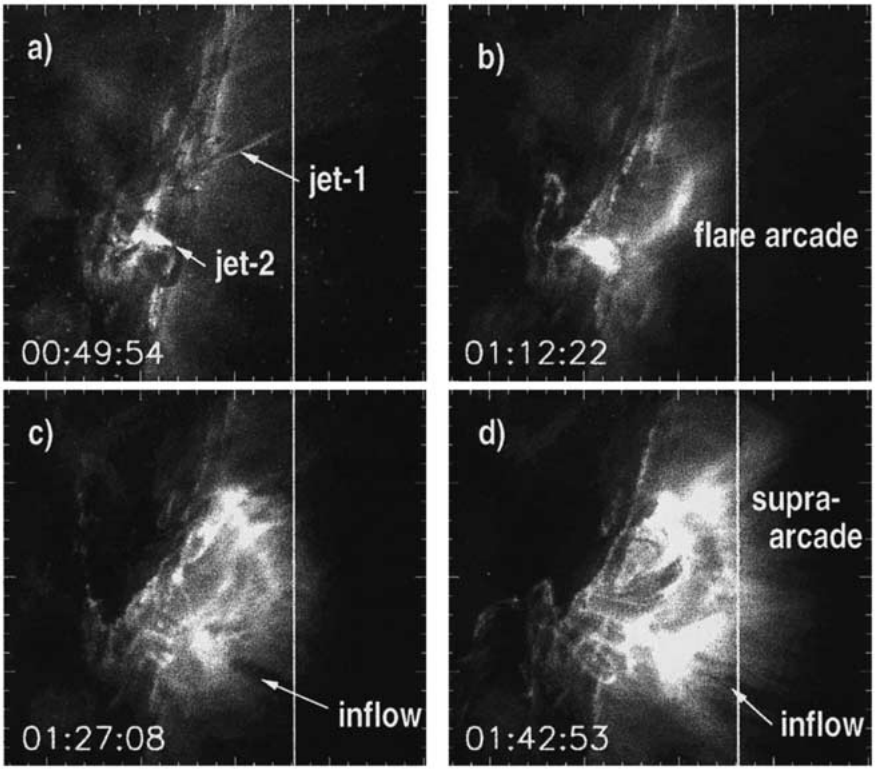

Figure 1. TRACE 195 Å filter images of the flaring region showing (a) the onset phase, (b) the initial flare arcade, (c) the beginning of the inflow phase, (d) the full extent of the supra-arcade. The position of the SUMER slit is shown with a *vertical white line*. The TRACE image FOV is 225×200 arc sec^2.

Similar dark sunward flows have been seen between 2.5–5 $R_\odot$ in white-light LASCO images (Sheeley and Wang, 2002). In these images brightness directly reflects the electron density structure of the corona, making their interpretation more straightforward than EUV or soft X-ray images. Sheeley and Wang (2002) see that the dark trails form after and behind a barely visible density enhancement. They think that the dark trails are a wake behind a falling structure.

On 21 April 2002, a spectacular post-flare coronal arcade with supra-arcade fan and inflows was observed on the south-west limb of the Sun. It was also associated with a large CME. The flare and CME were observed by many instruments, including RHESSI, TRACE and SOHO/EIT, SUMER, UVCS, and LASCO (Wang *et al.*, 2002; Caspi, Krucker, and Lin, 2002; Gallagher *et al.*, 2002; Gallagher, Lawrence, and Dennis, 2003; Dobrzycka *et al.*, 2003). The TRACE images in Figure 1, illustrate the initial stages of evolution, before and during the inflow phase. The arcade formed about 20 min after flare onset. It rapidly developed a supra-arcade structure, stretching to a height of over 100 Mm. Dark sunward moving trails can be seen against the bright EUV arcade emission in Figures 1(c) and 1(d).

The spectrometer SUMER obtained a time series of spectra in the lines C II, Fe XII, and Fe XXI of the flare supra-arcade structures. The cadence was short enough to see different sections of the dark inflows as they cross the position of the SUMER slit. Therefore a careful analysis of the spectra has the potential to unveil the origin of the dark flows. This paper presents a first analysis of the spectra at the time of the inflows and is directed at resolving the cause of the darkness: dense, cold absorbing plasma, or plasma voids.

In an accompanying paper (Innes, McKenzie, and Wang, 2003) a second aspect of the spectra, 1000 km s^{-1} flows in the Fe XXI line associated with the dark inflows, is reported. A third paper is planned to discuss the structure and oscillations seen in the TRACE images of the dark inflows. Models of the inflows (cf., McKenzie and Hudson, 1999; McKenzie, 2000; Sheeley and Wang, 2002) will be discussed in a subsequent paper.

2. Observations and Data Analysis

The flare was an X1.5, two-ribbon, CME-associated event on the west limb of the Sun and it lasted about 15 hours (Gallagher *et al.*, 2002). The first X-ray signature was at 00:43 UT, 21 April 2002, from a position near the footpoint of a jet-like structure in AR 9906, marked 'jet-2' in Figure 1(a). Almost simultaneously, a faint loop structure was seen expanding through the corona (Figure 2(a)) with a velocity of 120 km s^{-1} at a height of 100 Mm (Gallagher, Lawrence, and Dennis, 2003). This loop has been linked to the CME, traveling with a plane-of-sky speed 2500 km s^{-1} by the time it reached the LASCO field of view (2.2 $R_{\odot}$). It is one of the fastest CMEs ever seen. Sunward flows started to be seen against the bright arcade emission about 20 min after the loop ejection and they lasted about 1.5 hours. They produce dark channels in the EUV images (Figures 1(c) and 1(d) which have, in the difference images (Figure 2(b–d)), dark tips on their sunward end.

SUMER (Wilhelm *et al.*, 1995, 1997; Lemaire *et al.*, 1997) was pointing at a 4×300 arc sec^2 long, narrow strip of the solar corona about 100 arc sec above the limb centered at Sun co-ordinates 981,−184. Its position is marked as a vertical white line in Figures 1 and 2. Stigmatic images were taken of the C II 1335 Å ($T \sim 4 \times 10^4$ K), Fe XII 1349 Å ($T \sim 10^6$ K), and Fe XXI 1354 Å ($T \sim 10^7$ K) lines with a cadence of one image per 50 s. The contribution functions computed using CHIANTI (Dere *et al.*, 1997) of the three lines are shown in Figure 3. For most of the time, narrow spectral windows of width 2 Å centered on each of the lines were transmitted. Each hour a full spectral window from 1333–1373 Å was transmitted. Direct measurement of the line intensities can give constraints on the plasma emission measure at various temperatures using a model of the ionization and the element abundances. The line shifts give constraints on the plasma flow velocities.

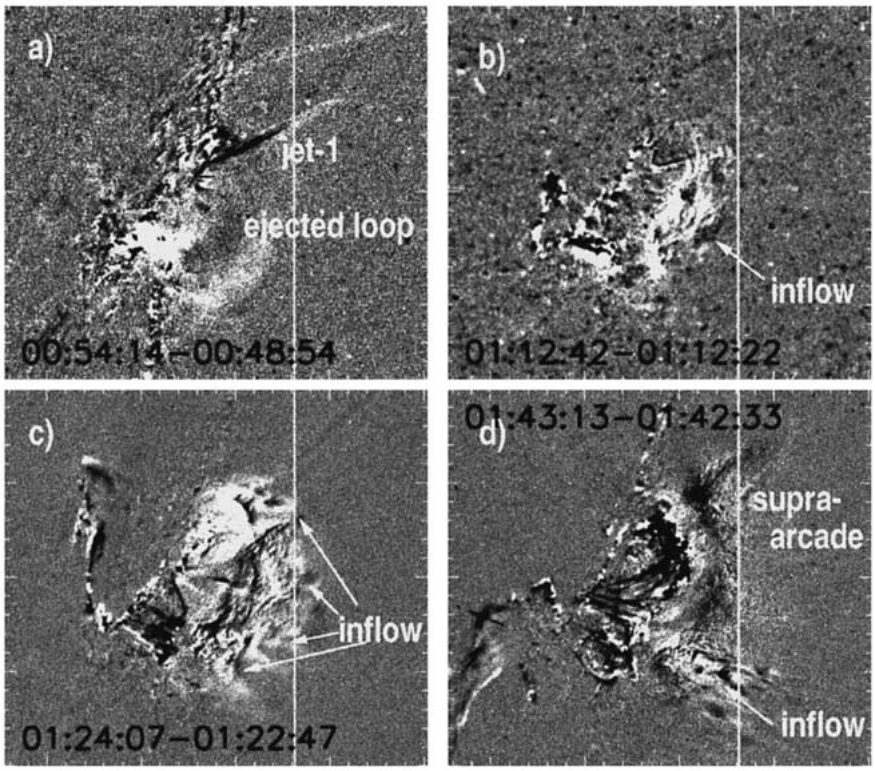

Figure 2. TRACE 195 Å difference images of the flaring region at times corresponding to those in Figure 1. The difference images are between the marked times. White indicates an intensity increase. Signs of inflow to the arcade top are visible as patches of dark at the top of the flare arcade in (b–d). The position of the SUMER slit is shown with a *vertical white line*. The TRACE image FOV is 225×200 arc sec^2.

The continuum emission around each line is a combination of first- and second-order radiation and may provide valuable clues to the origin of the dark EUV flows. In the wavelength region observed, the first-order ($\sim$ 1350 Å) emission is above the hydrogen Lyman limit and the second order ($\sim$ 675 Å) is below. So second-order photons are absorbed by H I along the line of sight and the first order are not. Thus, cold material along the line of sight may show up as a decrease in the second- to first-order continuum ratio.

The two orders can be disentangled by using the known detector response. As described by Wilhelm *et al.* (1997), the central part of the SUMER detector is coated with KBr. This essentially increases the detector sensitivity to photons by about an order of magnitude at wavelengths greater than 1100 Å. For example, at 1350 Å the KBr is almost 20 times more sensitive than the uncoated part of the detector. At wavelengths less than about 800 Å both the bare and the KBr are comparable. For comparison of first- and second-order continuum, one needs

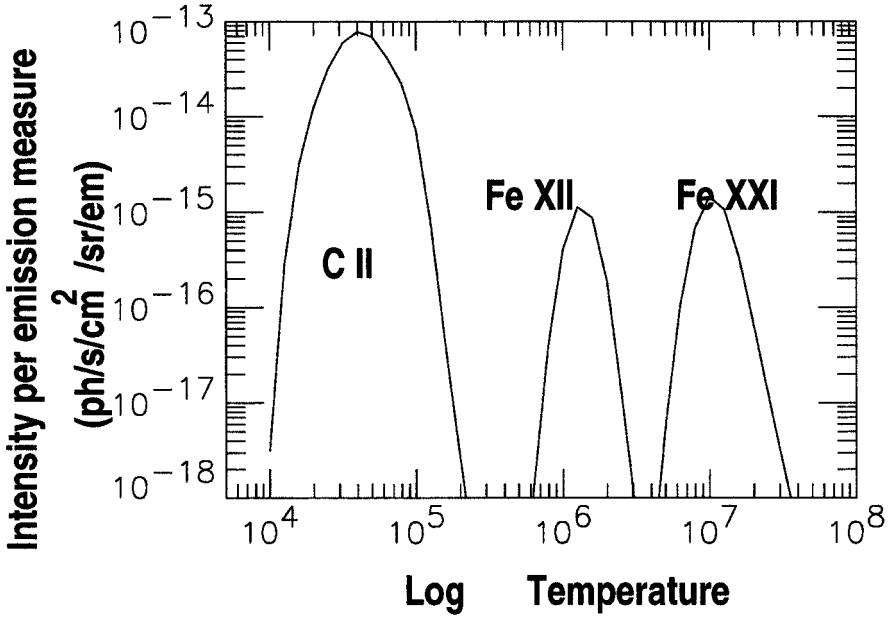

Figure 3. Line-intensity contribution functions for the lines observed by SUMER. Ionization equilibrium and Sun coronal abundances have been used.

observations on both the coated (KBr) and uncoated (bare) part of the detector. The C II was on the bare part of the detector and the Fe XII was on the KBr. As can be seen in Figure 4, the continuum around the C II is appreciably below the continuum around the Fe XII and Fe XXI. For each window, there is an equation relating the observed count rate to the first- and second-order intensities, $I_{\rm I}$ and $I_{\rm II}$, and the effective areas of the detector on the KBr and bare parts of the detector, $R_{\lambda}^{\rm KBr,bare}$, at the observed wavelengths. The equations for the counts on the KBr and bare are

$$C^{\rm KBr} = I_{\rm I} R_{1350}^{\rm KBr} + I_{\rm II} R_{675}^{\rm KBr} \tag{1}$$

and

$$C^{\rm bare} = I_{\rm I} R_{1335}^{\rm bare} + I_{\rm II} R_{667}^{\rm bare}. \tag{2}$$

The R's are given by the SUMER SolarSoft (Freeland and Handy, 1998) routine *radiometry*, so the equations can be solved to obtain $I_{\rm I}$ and $I_{\rm II}$.

C II is a doublet and except for a few transient events, the emission is stray light from the disk. It results in two faint emission lines along the spectrometer slit (Figure 5(a)). The positions of the lines do not change although their strength can vary a bit depending on the active-region disk brightness. We, therefore, average the intensity from specific pixels either side of the lines to compute the continuum. The pixels chosen to obtain continuum levels around the C II on the bare part of the detector are shown in Figure 5(a). In regions of bright coronal C II emission,

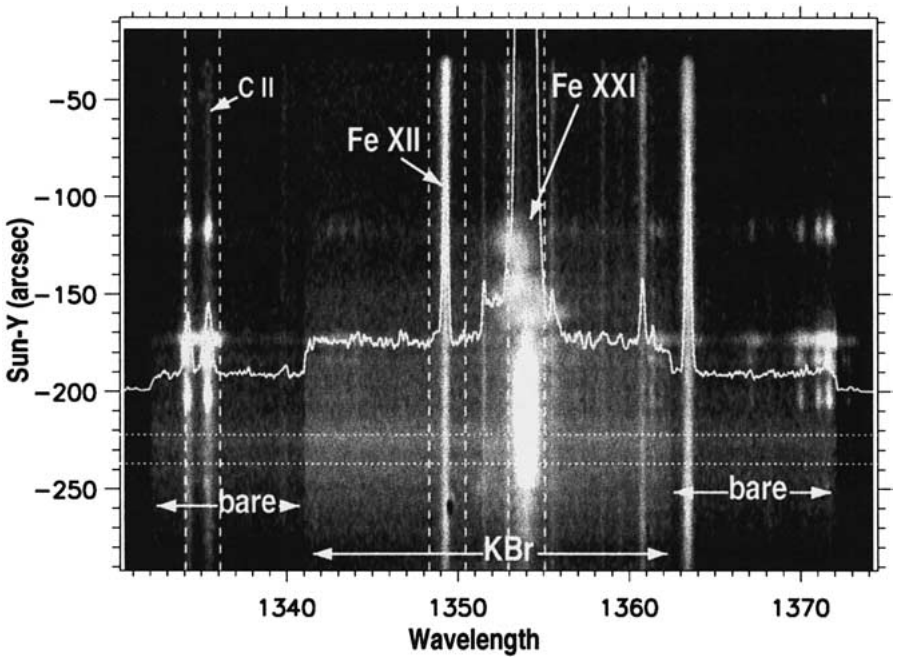

Figure 4. The SUMER spectrum taken at 01:26:33 UT, showing the change in detector sensitivity due to the KBr coating on the middle section. The profile is the spatially integrated emission between the *dotted lines*. The *dashed lines* show the three spectral regions transmitted throughout most the observing sequence.

the C II line wings spread into these continuum windows and the continuum will be over-estimated. For the most part, however, the C II is simply stray light and the line profiles are as shown in Figure 5(a). The pixels used to obtain the continuum count rate on the KBr coated part, around the Fe XII, are shown in Figure 5(b). Here we make a distinction between continuum on the blue and red side of Fe XII. As will be seen, there are phases in the evolution when the red-to-blue intensity ratio changes due to Fe XII and/or Fe XXI line emission shifting into one or the other of the continuum windows (see also Paper II).

The SUMER spectra have been divided by the most recent flat field, taken in November 2001. There is some evidence that this no longer represents the present small-scale structure of the detector so that caution must be exercised when interpreting stucture with a regular 5–6 pixel pattern. The other important correction applied to the SUMER data was the geometric correction which converts the raw 'inverse cushion' images to 'rectangular grid' images. The standard corrections for deadtime and local gain were also applied.

TRACE 195 Å images were obtained at full resolution (pixel size 0.5 arc sec) and with a cadence of approximately one image per 20 s. The main lines in this window are the 10^6 K Fe XII line at 195.1 Å and the 2×10^7 K Fe XXIV line at 192 Å. At high temperatures there is also strong bremsstrahlung continuum emission. There

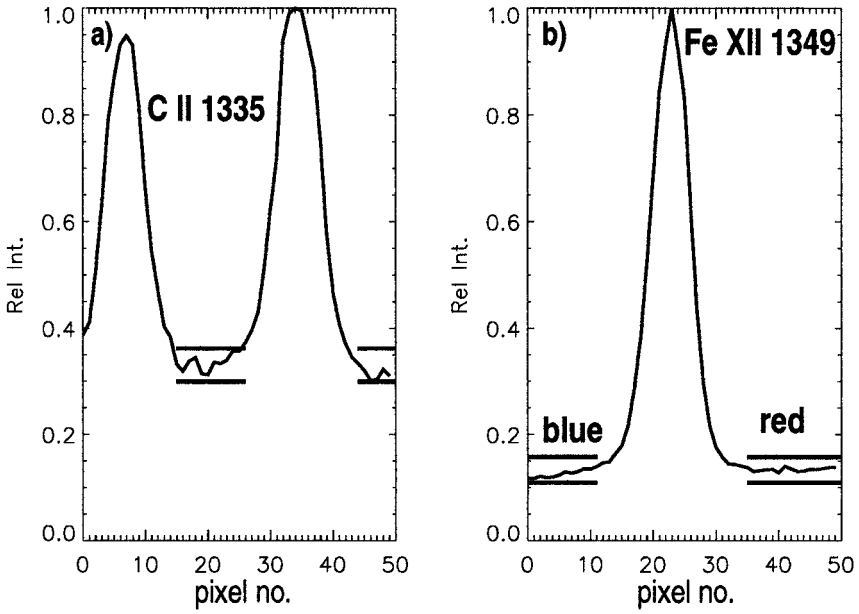

Figure 5. The average line profiles in the (a) C II and (b) Fe XII windows. The pixels used to estimate the continuum are marked with *solid horizontal lines*. As discussed in the text, the continuum on the *left* (marked *blue*) and *right* (marked *red*) of the Fe XII line behave differently.

were short interruptions in TRACE data around 00:50, 01:10, 01:40, and 02:00 UT. The images have been processed with the SolarSoft routine *trace_prep* to remove the dark pedestal and CCD characteristics.

Images at 304 Å, 171 Å, 195 Å, and 284 Å were obtained by EIT between 01:00 and 01:20 UT. The images at 171 Å, 195 Å, and 284 Å show the same flare arcade structures as the TRACE image. The 304 Å image shows colder loops extending into the corona at 01:19 UT at the position of bright C II emission in the SUMER spectra. The 304 Å image was calibrated using the SolarSoft routine *eit_prep*.

The TRACE, EIT and SUMER images were first co-aligned to within 5 arc sec using the given coordinates and pixel sizes in the image headers. Then, within that range, we adjusted the overlay for the best correspondence of the emissions. Using TRACE and SUMER time series between 00:30 and 04:00 UT, co-alignment to within 1 arc sec was achieved.

3. SUMER: Time–Space Evolution of the Arcade

The time variations of intensities in the three SUMER windows are shown in Figure 6, along with the corresponding time–space map of TRACE intensity. The TRACE image is constructed by extracting the time series of 195 Å intensities at the position of the SUMER slit (Sun-X $= 981$ and $-346 \leq$ Sun-Y≤ -50). Each

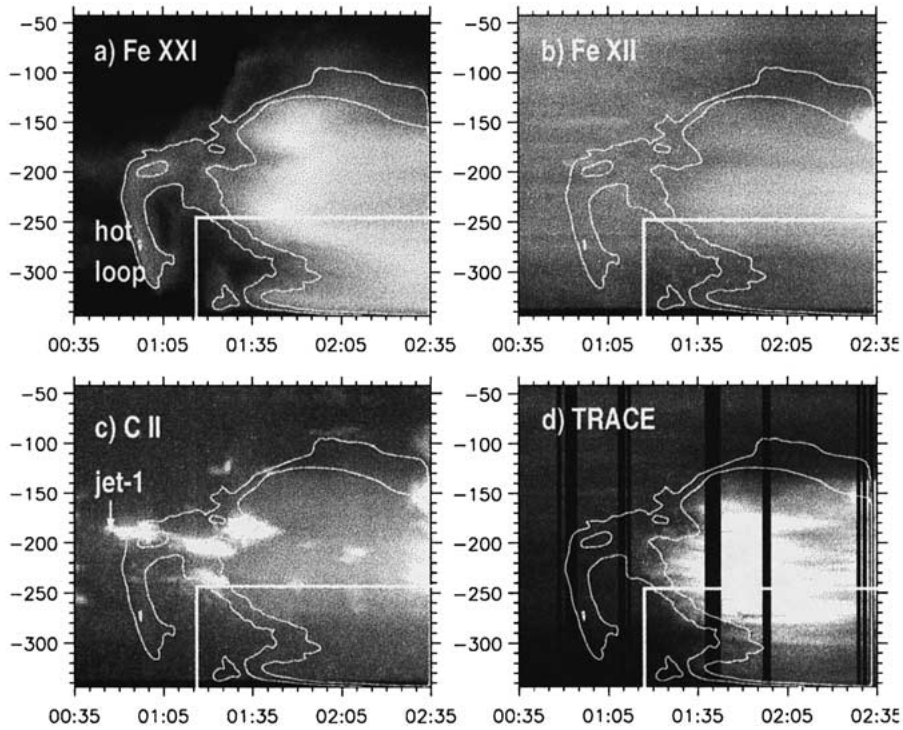

Figure 6. The time evolution of SUMER intensities obtained at the position marked in Figure 1, together with the TRACE 195 Å intensity evolution at the same position. The *white contours* outline the main Fe XXI emission. All SUMER intensities are integrated over the 2 Å wide windows. The intensities are displayed with a logarithmic scale. The *white rectangle* shows the position of the dark inflows analyzed in Section 4.

of the SUMER frames in this figure is the sum of continuum and line intensity. The two components can be separated in the C II and Fe XII windows (Figure 7) but the Fe XXI line is so broad that it essentially fills the whole 2 Å window and so the components cannot be separated. The Fe XXI hot, hook-shaped feature is, as explained in Wang *et al.* (2002), the rising loop in Figure 2(a). The 'jet-1' (see Figures 1 and 2) is only seen in the C II image so it must be mostly cold material.

The intensity in the Fe XII window increases after 01:25 UT when the flare arcade rises into the SUMER field of view. This general pattern is reflected in the TRACE. The TRACE images however show more contrast. Of particular interest are the dark channels around (01:40 UT, −300) cutting into the bright arcade emission.

3.1. THE Fe XII WINDOW

After 01:15 UT, much of the emission in the Fe XII window is continuum. The continuum is bremsstrahlung emission from the hot flare arcade. The separate

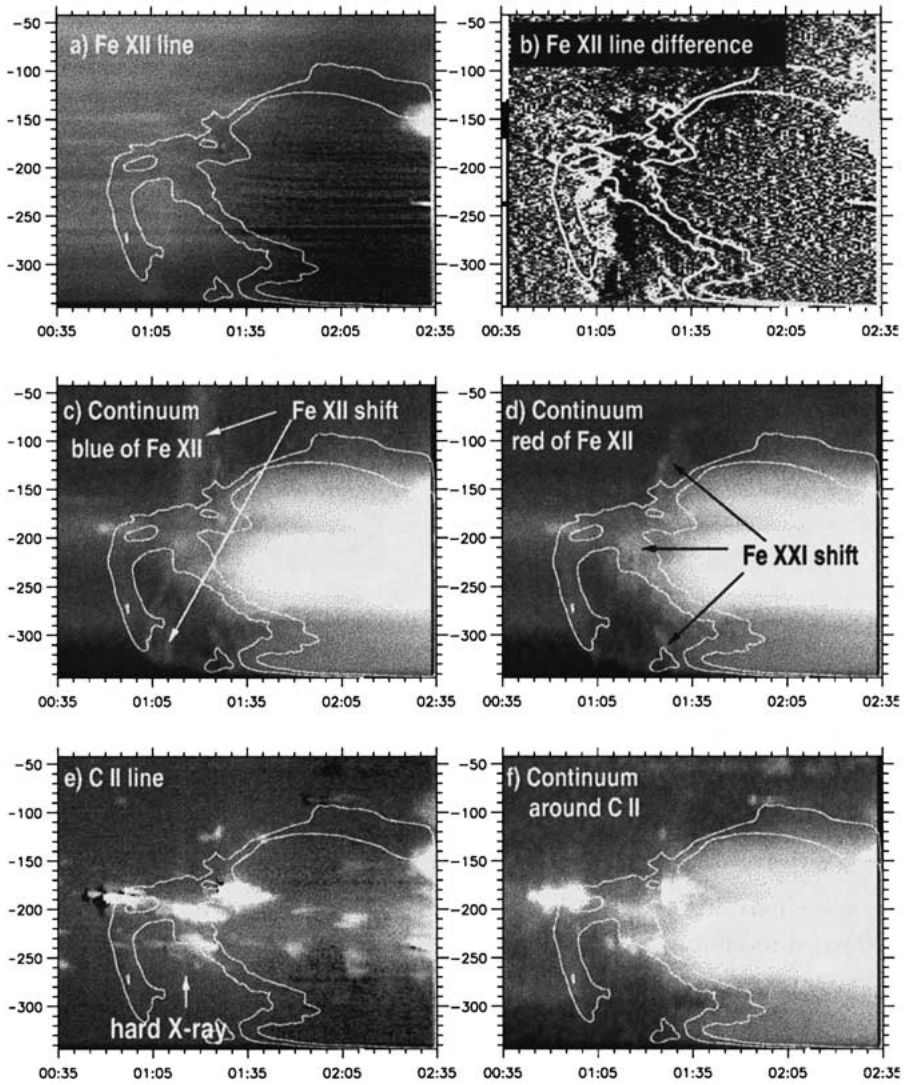

Figure 7. The time evolution of the SUMER line intensities and continuum around the line, scaled logarithmically. Contours outline the position of main Fe XXI emission as in Figure 6. (a) Fe XII line intensity. (b) Fe XII running difference with 5 min time lag. (c) Continuum on the blue side of the Fe XII line. Features of high Fe XII line shift are marked. (d) Continuum on the red side of the Fe XII line. Features of high Fe XXI line shift are marked. (e) C II line intensity. f) Continuum around C II.

Fe XII line and continuum intensities are shown in Figure 7(a–d). Here, the line emission is that remaining after continuum subtraction (Section 2).

Fe XII line emission decreased suddenly from the whole slit area at about 01:10 UT (Figure 7(b)). At the same time, Doppler-shifted Fe XII is picked up in the continuum on the blue side of the line. It is marked 'Fe XII shift' on Figure 7(c).

The Doppler shift associated with the front is at least 250 km s^{-1} and it moves up the slit with a speed of 600–1000 km s^{-1}. Unfortunately there is a TRACE data gap at exactly this time and it is not possible to see the origin of this front. It may be related to the CME. The continuum on the red side of the line is shown in Figure 7(d). Here the faint features, seen before the arrival of the arcade continuum, are believed to be due to Fe XXI line emission with Doppler shift ~ 1000 km s^{-1} (Paper II).

3.2. THE C II WINDOW

For the interpretation of the dark flows, the C II line emission is probably most interesting. The separate line and continuum contributions to the C II window are shown in Figure 7(e) and 7(f). There are four main C II emission structures in the first hour of the flare. The first is related to 'jet-1'. The second and third, as shown in the EIT He II 304 Å image taken at 01:19:25 UT, are also related to disk loop or jet-like structures. Figure 8 shows there were cold structures reaching as far out as the SUMER slit at this time. SUMER spectra show they formed at this height around 01:10 UT and lasted until 01:30 UT.

The amount of material in the cold structures along the line of sight can be estimated from the C II and EIT 304 intensities. As seen in Figure 8, the spatial overlap between the two is very good and it is quite likely that the two lines are essentially coming from the same plasma. A lower limit to the emission measure can be obtained by assuming the line intensity of any line is coming from plasma at the peak of the line's contribution function. The EIT 304 band is dominated by He II at temperatures below 10^5 K, and the peak in the He II contribution function in ionization equilibrium is at 8×10^4 K. The C II 1335 Å band has its peak contribution at 4×10^4 K. The emission measure in Figure 8 for the 304 band is computed with the SolarSoft routine *eit_flux*, assuming a temperature 8×10^4 K. The emission measure of the C II is determined from the contribution function (Figure 3) at a temperature 4×10^4 K. It is amazing that the two emission measure estimates (Figure 8(b)) are within a factor two of one another. The uncertainty associated with emission measure modeling at these low temperatures must be at least this big when one takes into consideration the uncertainty in the abundances, the ionization, the thermal mixing, etc. If this emission measure is correct, then with a structure width, 15 arc sec, the electron density would be 10^9 cm^{-3}. The other C II structures in the SUMER spectrum are found at similar locations. They are most likely also related to cold loops in the corona.

Another interesting feature of the C II intensity is the brightening along the length of the slit at 01:15 UT. This is exactly the time of the first hard X-ray burst recorded by RHESSI (Caspi, Krucker, and Lin, 2002; Gallagher *et al.*, 2002). It is seen in no other line or in the continuum. It is either caused by an increase in the C II stray light or resonance scattering in the corona.

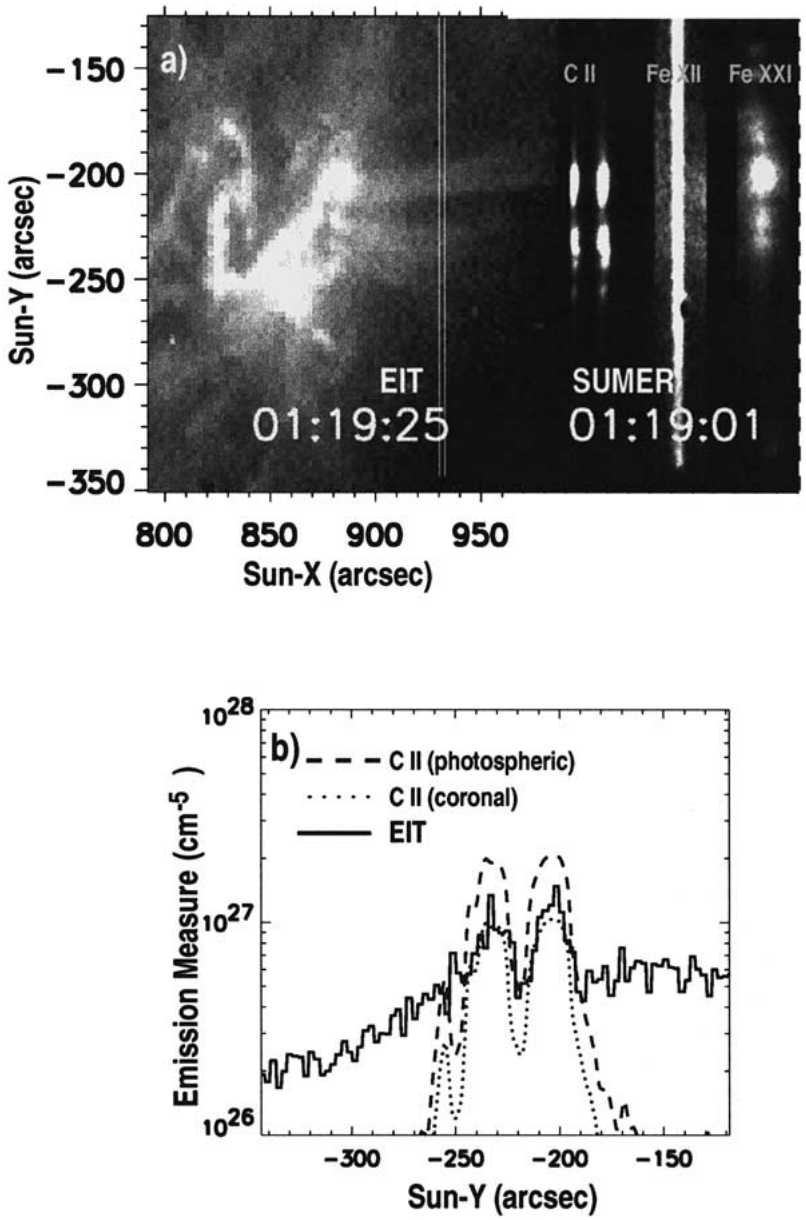

Figure 8. SUMER spectra at the time of the EIT 304 Å image showing the C II structures in the active region. (a) EIT 304 Å image aligned with the SUMER C II, Fe XII, and Fe XXI spectra. (b) Emission measure from the EIT 304 Å intensities at the position of the SUMER slit compared to the emission measure computed from C II intensities assuming photospheric and coronal abundance.

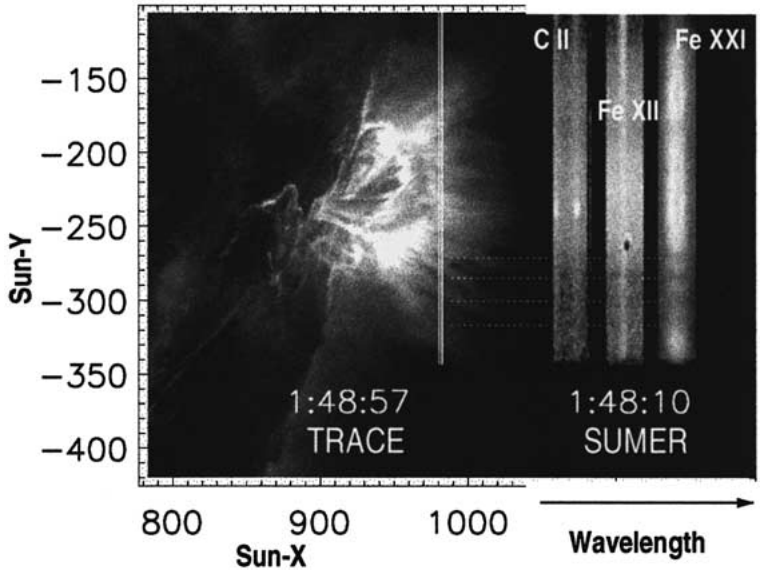

Figure 9. SUMER spectra co-aligned to one of the TRACE images at the time of several inflows in the south. The *vertical white line* on the TRACE image is the SUMER slit position. *Dotted lines* connect the dark TRACE inflows to the corresponding positions in the SUMER spectra. The *black dot* in the middle of the Fe XII window near Sun-Y $= -270$ is a detector artifact.

4. Structure and Density of Dark Inflows

Inflows are seen in TRACE images across the whole region from about 01:10 UT onwards. The most spectacular tracks in the TRACE images are seen in the south after 01:30 UT. Figure 9 shows co-aligned TRACE and SUMER spectra at the time of the southern inflows. The dark TRACE tracks are also seen in the UV continuum and in Fe XXI observed by SUMER but they are not seen in either the C II or the Fe XII line emission. Therefore we can rule out dense plasma structures with temperature greater than 10^4 K.

The UV continuum can be used to investigate the possibility that they are caused by even colder plasma. Because the count rates in the continua are low the spectra have been averaged over four space and two time bins. Some of the structure is therefore lost. The wavelength windows used to obtain the continua are shown in Figure 5. The Fe XII continuum has been divided into red and blue because line shifts from Fe XXI and Fe XII cause differences in the two continuum levels.

We concentrate on the time of very clear dark inflow tracks in the south. During this phase of the arcade evolution, the arcade is rising up to the height of the SUMER slit. SUMER and the corresponding TRACE space–time images of the inflows (white box in Figure 6) are shown in Figure 10. The TRACE image (Figure 10(a)) shows several dark channels in the bright arcade emission. The northern inflow, 'F1', is interesting because it appears at this height inside the arcade emis-

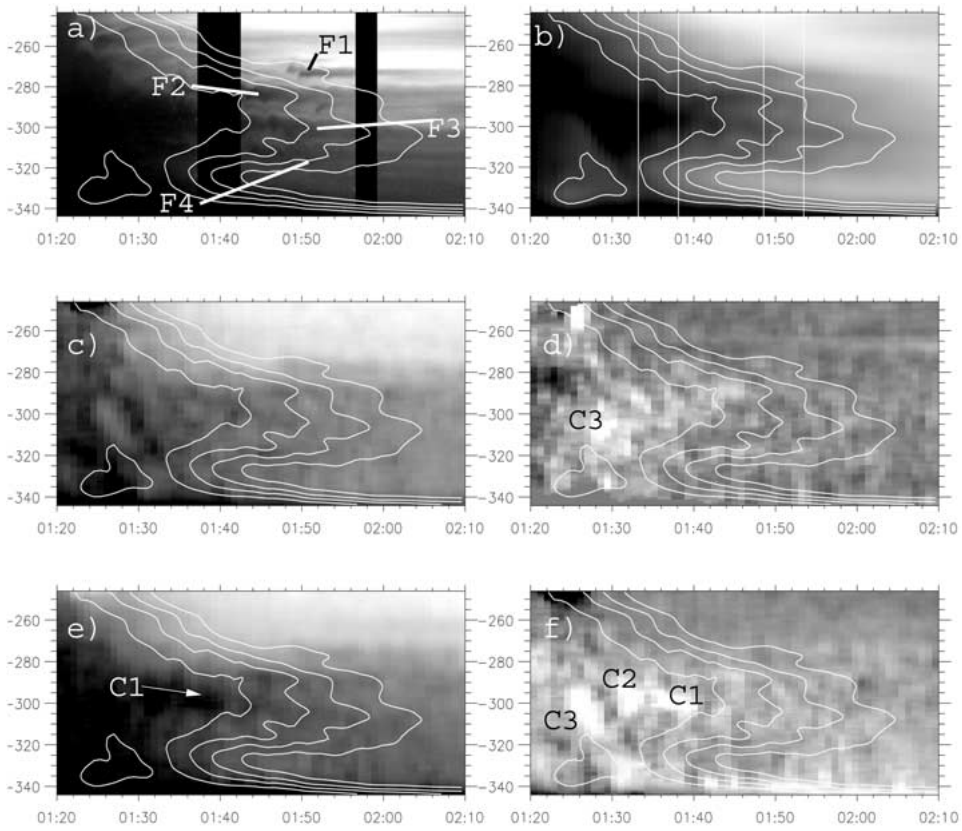

Figure 10. Time–space maps near inflows (a) TRACE. (b) Fe XXI. (c) First-order continuum. (d) Ratio of the continuum red and blue of Fe XII, scaled logarithmically between 0.25 and 4 (*white*). (e) Second-order continuum. (f) The ratio 3.5 times the first order continuum to the second order continuum, scaled logarithmically between 0.25 and 4. The ratio for bremsstrahlung emission is 1. The contours outline the Fe XXI emission. The *white vertical lines* in (b) show the time intervals used to create the plots in Figures 12 and 13. The flows F1-F4 are shown in Figure 12 and the channel, C1, is shown in Figure 13.

sion. It is an inflow falling through existing hot arcade plasma. The other inflows appear as dark channels holding off the arcade emission at their positions. There seem to be three separate inflows, 'F2, F3, F4'. The contours in Figure 10 are the Fe XXI flux distribution, displayed in Figure 10(b). The dark Fe XXI channels correlate almost exactly with those in the TRACE image.

Figure 10(c) shows the first order continuum, computed using the continuum level on the blue of the Fe XII line and the continuum in the wing of C II. Here the contrast across the four inflows does not appear to be so well pronounced as in Fe XXI and TRACE. The next figure (Figure 10(d)), is the ratio of the Fe XII continuum intensity on the red and blue side. It is mostly featureless (gray). The

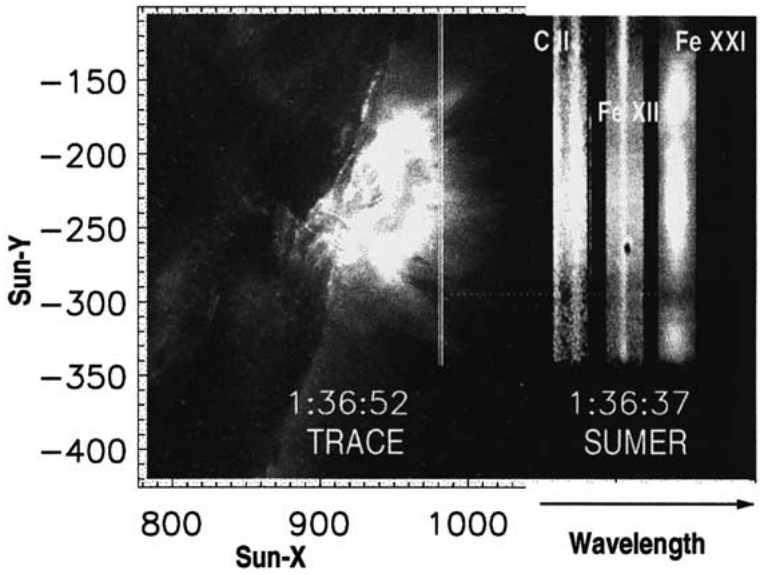

Figure 11. SUMER spectra co-aligned to the TRACE image at the time of unusually low second-to-first-order continuum ratio. The *vertical white line* on the TRACE image is the SUMER slit position. A *dotted line* connects the dark TRACE inflow to the region of dark continuum around C II (the second order – see text).

white spot,'C3', at (01:30 UT, −310) has been pointed out in Figure 7 as a 'Fe XXI shift' region.

The last two frames of Figure 10 are critical for interpretation of the inflows. The first, Figure 10(e), is the second-order continuum. The second is the ratio of the first-order continuum multiplied by a factor 3.5 to the second-order continuum, scaled logarithmically between 0.25 and 4. This has been done in order to compare directly with a bremsstrahlung source spectrum. At $T > 3 \times 10^6$ K, the continuum beyond 600 Å is essentially all bremsstrahlung (Landini and Monsignori Fossi, 1990) and the intensity ratio between the first and second-order changes between 3.4 ($T = 5 \times 10^6$ K) and 3.6 ($T = 5 \times 10^7$ K) according to the routine *freefree* in the CHIANTI software package. If the emission were pure bremsstrahlung, the image would be gray (ratio = 1.0). The image becomes grayer and more uniform across the region of bright continuum along the top. The bottom half of this image is distinctly whiter. The ratio is typically 1.2, implying that there is slightly more first-order continuum than expected for a bremsstrahlung source. There are, however, three regions with a ratio greater than 4, marked 'C1, C2, C3'. At 'C3' there is also a significant difference in the continuum level on the blue and red side of the Fe XII line (Figure 10(d)). This suggests that the first-order continuum may be increased due to Doppler-shifted Fe XXI (Paper II). The large first-to-second-order ratio at 'C1' and 'C2' cannot be so easily explained as an increase in the first-order continuum. The more likely explanation is absorption of short wavelength,

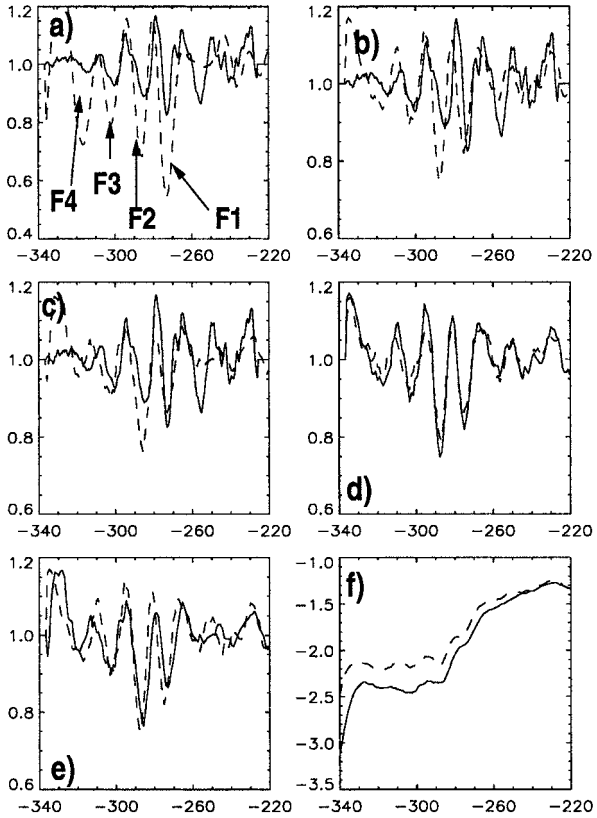

Figure 12. Flux across the dark inflows in Figure 10, averaged between 01:48 and 01:53 UT. (a) TRACE and Fe XXI (*dashed*). (b) TRACE and first-order continuum (*dashed*). (c) TRACE and second-order continuum (*dashed*). (d) Continuum blue of Fe XII and red of Fe XII (*dashed*). (e) First-order continuum and second-order continuum (*solid*). (f) Second-order continuum (*solid*) and 3.5 times the first-order continuum. The fluxes in (a–e) have been normalized to the smoothed value. (f) shows log intensity in W sr^{-1} $m^{-2}Å^{-1}$.

second-order, photons by cold intervening material. There is a dark channel at 'C1' in image Figure 10(e). In the SUMER spectrum, Figure 11, it can be seen as a dark region in the C II continuum at Sun-Y $= -300$ and in the Fe XXI, but not in the Fe XII continuum. As explained in Section 2, the KBr coating on the central part of the detector increases its sensitivity to photons with wavelength greater than 800 Å. There is more than a factor 10 difference in the sensitivity of the KBr and bare part of the detector to first-order photons. For spectra, like bremsstrahlung, with intensity inversely proportional to the wavelength squared, the observed continuum emission on the bare part is nearly all second order, and that on the KBr is about half second order and half first order.

Two time intervals have been selected for more detailed investigation. The intervals are drawn in Figure 10(b). The earliest, between 01:33 and 01:38 UT, covers

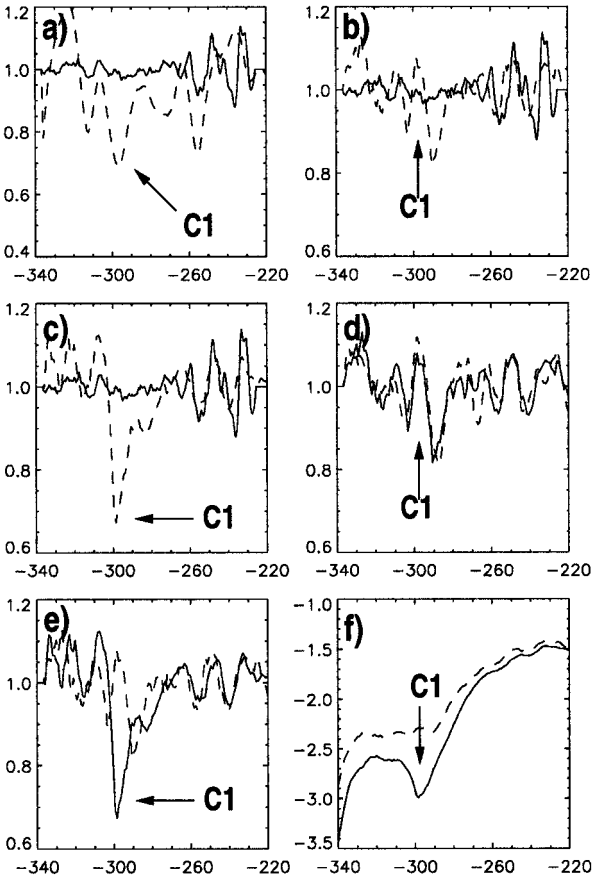

Figure 13. Fluxes across the dark channel in Figure 10, averaged between times 01:33 and 01:38 UT. The fluxes are the same as in Figure 12.

the dark track, 'C1'. The later one between, 01:48 and 01:53 UT, covers a time when the four inflows are crossing the SUMER slit position. The time-averaged fluxes at these two times are shown in Figures 12 and 13.

Figure 12 shows the fluxes at the later time, when there are four inflows. All four, 'F1–F4', show up clearly in the Fe XXI, the first- and second-order continuum, and TRACE (Figure 12(a–c)). Figure 12(d) compares the continua on the red and blue side of Fe XII. Again the important figures for the absorption are the last two. Figure 12(e) compares the structure of first- and second-order emission across the region. Both the first and second order decrease by about the same amount across the flows. This implies that at this time and height, the dark channels are caused by less emission measure, not by absorption along the line of sight. Figure 12(f), compares the observed fluxes to bremsstrahlung emission. The dashed line is 3.5 times the first-order flux and the solid line is the second-order flux. The two lines

TABLE I

H I column density.

Time (UT)	Position	Ratio	τ	$n_{\rm H}\ dl$ (cm^{-2})
01:36	−300	4.4	1.5	6×10^{17}
01:36	−250	1.1	0.1	4×10^{16}
01:50	−300	1.6	0.5	2×10^{17}
01:50	−250	1.1	0.1	4×10^{16}

would overlap if it was pure bremsstrahlung. Across the flows the difference is about 0.2, corresponding to a ratio of about 1.6.

At the earlier time, 01:33 to 01:38 UT, the TRACE images show a broad dark channel in the arcade emission at the height of the SUMER slit and Sun-Y = −300 (Figure 11). This channel is not seen in the SUMER first-order continuum (Figure 10(c)) but it is seen in the Fe XXI (Figure 10(b)) and second-order continuum (Figure 10(e), marked 'C1'). The implication is that the bremsstrahlung emission from the hot arcade top is approximately uniform but there are changes in temperature and absorption in the region of the dark TRACE channel. The plots in Figure 13 show the same. There is a dip in the Fe XXI (Figure 13(a)) and second-order continuum at 'C1' (Figures 13(c), 13(e), and 13(f)). The second-order intensity is a factor 5 less than expected for a bremsstrahlung source and the observed first order continuum intensity. This is only a lower limit because the continuum around the C II is virtually non-existent.

Finally in this section, we compute the implied H I column density from the continuum ratios. The results are summarized in Table I. The logarithm of the ratio (3.5 times the first-order continuum flux to the second-order continuum) gives the optical depth τ. The column density, $n_{\rm H}\ dl$, is computed using the H I absorption cross section, 2.5×10^{-18} cm^2, at 670 Å (Rumph, Bowyer, and Vennes, 1994). These column densities are appropriate for cold neutral hydrogen absorbing radiation from hot background plasma. No allowance has been made for foreground emission (cf., Kučera, Andretta, and Poland, 1998). The analysis is aimed at determining whether the TRACE EUV dark structure is caused by plasma voids or absorbing material. The absorption cross section at 195 Å is approximately 2.5×10^{-19} cm^2, including contributions from H I, He I, and He II (Rumph, Bowyer, and Vennes, 1994). Since this is about an order of magnitude less than the cross-section at 670 Å, it seems very unlikely that the EUV darkening can be attributed to absorption. The only region where absorption may be responsible is the channel 'C1'. The column density given in Table I, is also too small to account for the EUV darkness but the column density may be much higher than the estimate because the counts in the continuum around C II are very few and have large uncertainty.

5. Conclusion

The dark inflows seen at 195 Å in TRACE were also seen in SUMER Fe XXI and UV continuum. These were not seen in C II and Fe XII. The ratio of the UV continuum longward and shortward of the Lyman limit indicate a small amount of plasma with temperature below 10^4 K. Only at one position is absorption of second-order photons associated with a dark Fe XXI channel. It is also seen as a broad dark channel reaching into the top of the TRACE arcade. The derived column density of H I is not enough to cause any observable dimming in the 195 Å. It is therefore our conclusion that the dark tracks are plasma voids and are not caused by intervening cold plasma clumps. Although it is tempting at this stage to model the inflows in terms of evacuated magnetic flux tubes or sunward-directed magnetic islands, we do not want to speculate until details of other SUMER observations (Paper II) and TRACE images have been analyzed.

Acknowledgements

These observations could not have been obtained without the help of the SUMER planners Cristian Vocks and Werner Curdt. We would also like to thank Hugh Hudson for his valuable comments and an anonymous referee for helpful criticism. The SUMER project is financially supported by DARA, CNES, NASA and the ESA PRODEX programme (Swiss contribution). SUMER and MDI are part of SOHO, the Solar and Heliospheric Observatory of ESA and NASA.

References

Caspi, A., Krucker, S., and Lin, R. P.: 2002, *American Geophysical Union, Fall Meeting 2002, abstract #SH52A-0465*, p. A465.

Dere, K. P., Landi, E., Mason, H. E., Monsignori Fossi, B. C., and Young, P. R.: 1997, *Astron. Astrophys. Suppl.* **125**, 149.

Dobrzycka, D., Raymond, J. C., Biesecker, D. A., Li, J., and Ciaravella, A.: 2003, *Astrophys. J.* **588**, 586.

Freeland, S. L. and Handy, B. N.: 1998, **182**, 497.

Gallagher, P. T., Lawrence, G. R., and Dennis, B. R.: 2003, *Astrophys. J.* **588**, L53.

Gallagher, P. T., Dennis, B. R., Krucker, S., Schwartz, R. A., and Tolbert, A. K.: 2002, *Solar Phys.* **210**, 341.

Innes, D. E., McKenzie, D. E., and Wang, T. J.: 2003, *Solar Phys.* **217**, 267. Paper II.

Kučera, T. A., Andretta, V., and Poland, A. I.: 1998, *Solar Phys.* **183**, 107.

Landini, M. and Monsignori Fossi, B. C.: 1990, *Astron. Astrophys. Suppl.* **82**, 229.

Lemaire, P., Wilhelm, K., Curdt, W., Schule, U., Marsch, E., Poland, A. I., Jordan, S. D., Thomas, R. J., Hassler, D. M., Vial, J. C., Kuhne, M., Huber, M. C. E., Siegmund, O. H. W., Gabriel, A., Timothy, J. G., and Grewing, M.: 1997, *Solar Phys.* **170**, 105.

McKenzie, D. E.: 2000, *Solar Phys.* **195**, 381

McKenzie, D. E. and Hudson, H. S.: 1999, *Astrophys. J.* **519**, L93.

Rumph, T., Bowyer, S., and Vennes, S.: 1994, *Astron. J.* **107**, 2108.
Sheeley, Jr. N. R. and Wang, Y. -M.: 2002, *Astrophys. J.* **579**, 874.
Wang, T. J., Solanki, S., Innes, D. E., and Curdt, W.: 2002, in H. Sawaya-Lacoste (ed.), 'Magnetic Coupling of the Solar Atmosphere', *Proc. IAU Colloq.* **188**, 607.
Wilhelm, K., Curdt, W., Marsch, E., Schuhle, U., Lemaire, P., Gabriel, A., Vial, J., Grewing, M., Huber, M. C. E., Jordan, S. D., Poland, A. I., Thomas, R. J., Kuhne, M., Timothy, J. G., Hassler, D. M., and Siegmund, O. H. W.: 1995, *Solar Phys.* **162**, 189.
Wilhelm, K., Lemaire, P., Curdt, W., Schuhle, U., Marsch, E., Poland, A. I., Jordan, S. D., Thomas, R. J., Hassler, D. M., Huber, M. C. E., Vial, J., Kuhne, M., Siegmund, O. H. W., Gabriel, A., Timothy, J. G., Grewing, M., Feldman, U., Hollandt, J., and Brekke, P.: 1997, *Solar Phys.* **170**, 75.